https://doi.org/10.22226/2410-3535-2022-4-451-456

Fracture features of impact samples of low-activation ferritic-martensitic steel EK-181 after high-temperature thermomechanical treatment

N. A. Polekhina[†,1], V. V. Linnik[1], I. Yu. Litovchenko[1], K. V. Almaeva[1],

V. M. Chernov[2], M. V. Leontieva-Smirnova[2]

[†]nadejda89tsk@yandex.ru

[1]Institute of Strength Physics and Materials Science of the Siberian Branch of the RAS, Tomsk, 634055, Russia
[2]A. A. Bochvar High-Technology Research Institute of Inorganic Materials, Moscow, 123098, Russia

A comparative fractographic investigation of fracture in the temperature range from −186 to 100°C of the Charpy impact samples is performed for the reactor low-activation ferritic-martensitic steel EK-181 after its high-temperature thermomechanical treatment (HTMT) and traditional heat treatment (THT). The mechanisms of steel fracture are revealed depending on the impact test temperature and treatment mode. On the upper and lower shelves of the impact toughness temperature curve, the steel fractures by the mechanism of transcrystalline ductile dimple fracture and transcrystalline quasi-cleavage, respectively. In the intermediate region (in ductile-brittle transition area), fracture occurs by a mixed mechanism. The transition temperature to the brittle state is determined, at which the proportion of ductile and brittle fractures is the same (after THT it is −3°C; after HTMT it is −14°C). It is established that HTMT significantly changes the type of fracture of the impact samples in comparison with THT. The microstructure formed during HTMT with hot deformation of austenite leads to the appearance of a crack-arrester type of delamination during the impact tests in the cold brittleness region, favoring an increase in the fracture toughness of the steel at a lower ductile-brittle transition temperature.

Keywords: ferritic-martensitic steel EK-181, ductile-brittle transition temperature, fracture mechanism, cleavage fracture, dimple fracture, delamination.

1. Introduction

Currently, with the advances in the nuclear industry, there is an increasing need for the development or improvement of the structural materials used for critical structural elements — claddings of fuel elements of fast neutron reactors and in-core devices of the thermonuclear reactors [1–4].

Among the promising classes of materials for these purposes are heat-resistant low-activation ferritic-martensitic steels with the chromium content of 9–12%, since they have a number of attractive properties [1,2,5,6]. Their main advantage, in comparison with the currently used austenitic steels, is a low tendency to void swelling during irradiation [1,6]. This allows significantly increasing the degree of the nuclear fuel burnout.

However, the ferritic-martensitic steels, being bcc materials, have a disadvantage due to their cold brittleness with the decreasing temperature and a rather low level of heat resistance [5–10]. These problems limit the lower and upper bounds of the operating temperatures range for such materials in the reactor core. The solution of these problems may be found in the development of optimal treatment modes or the selection of optimal compositions of ferritic-martensitic steels [2,4,11].

The Russian representative of the ferritic-martensitic reactor steels is a low-activation heat-resistant 12% chromium ferritic-martensitic steel EK-181 (Fe-12Cr-2W-V-Ta-B). To expand its operation temperature range, the modes of modifying treatments have been proposed [12–15]. It was shown in [13,14] that a significant (by ≈20%) increase, relative to the traditional heat treatment, in the strength properties of steel in a wide (from −196 to 800°C) temperature range can be achieved using a high-temperature thermomechanical treatment (HTMT) with deformation in the austenitic region. HTMT contributes to the formation of a banded ultrafine-grained structure of steel EK-181 with a high density of dislocations and nanosized particles of vanadium carbonitride [12–14]. In addition, according to the results of impact tests, this treatment also provides an increase in the impact toughness [15]. To understand the reasons for this behavior of the steel, it is of interest to identify the regularities and mechanisms of fracture of steel samples with different levels of strength properties in the cold brittleness area. In accordance with the above, in this paper we carry out a comparative study of the fracture behavior of impact samples (which are destroyed in the low-temperature range) of the low-activation ferritic-martensitic steel EK-181 after high-temperature thermomechanical treatment, which has proved its good promise, and a traditional heat treatment.

2. Materials and experimental method

The elemental composition of steel EK-181 is presented in Table 1. The traditional heat treatment of the steel consists of quenching from 1100°C (holding for 1 h) and tempering at T = 720°C (holding for 3 h). High-temperature thermomechanical treatment (HTMT) was carried out according to the following mode: heating to T=1100°C (holding for 1 h), hot plastic deformation by rolling in the austenitic region to a value of ε ≈ 50%, followed by quenching in water and tempering at 720°C (holding for 1 h).

Fractographic studies were carried out by scanning electron microscopy (Tescan MIRA 3 LMU) on Charpy-type impact test samples (3×4×27 mm in size with a V-notch 1 mm deep, notch tip radius R = 0.1 mm) of steel after THT and HTMT, destroyed in the temperature range from −186 to 100°C [15]. The orientation of impact test samples relative to the rolling direction is shown in Fig. 1.

The area fractions of the ductile and brittle components in the fractures of the samples tested at different temperatures were measured (according to the ASTM E23-05 standard). The temperature of the ductile-brittle transition (FATT, Fracture Appearance Transition Temperature) is defined as the temperature at which the fractions of brittle and ductile fractures are the same.

The ductile-brittle transition temperature (DBTT) was determined from the curve of the temperature dependence of impact strength as the midpoint between the maximum and minimum impact toughness values in the temperature range under study [15].

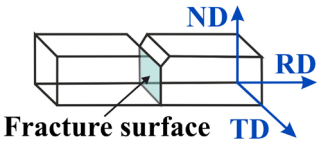

Fig. 1. (Color online) Orientation of the V-notch Charpy impact test sample to the rolling direction. RD — rolling direction, ND — normal direction, TD — transverse direction.

3. Results and discussion

In the structural states after THT and HTMT, steel EK-181 has a tempered martensitic structure typical for 9–12% chromium ferritic-martensitic steels (Fig. 2). The differences of the microstructure after HTMT from that after THT are as follows [8,12–14]: a decrease in the size of the steel grain-subgrain structure (grains of the prior austenite, ferrite, blocks and lamellae of martensite); an increase in the density of dislocations by several times; a decrease in the size and volume fraction of coarse $M_{23}C_6$ (M — Cr, Mn, W, etc.) particles, which are located mainly at the boundaries of the steel structural elements (Fig. 2 b); an increase in the volume fraction and dispersion of nanosized (diameter 5–10 nm) particles of MX carbonitride (M — V, Ti, Ta, etc., X — C, N), pinning the steel dislocation structure (Fig. 2 c).

Earlier [15] we studied the temperature dependence of the impact toughness of steel EK-181 after THT and HTMT (Fig. 3). It was shown [15] that HTMT results in a shift of the steel ductile-brittle transition temperature by several degrees

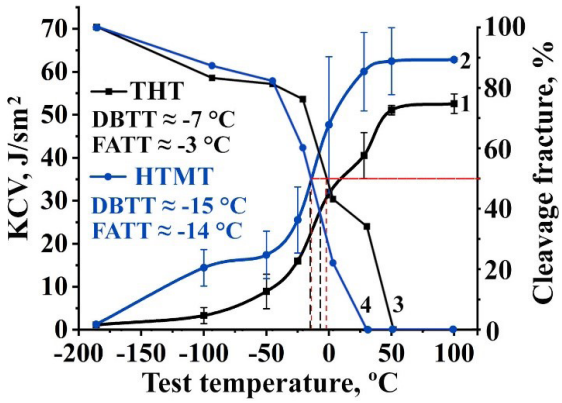

Fig. 3. (Color online) Temperature dependence of impact toughness (curves 1, 2) and brittle fracture area fraction (curves 3, 4) of EK-181 steel after THT (curves 1, 3) and HTMT (curves 2, 4) in the temperature range from −186 to 100°C. DBTT — Ductile-Brittle Transition Temperature. FATT — Fracture Appearance Transition Temperature.

Table 1. Elemental composition of EK-181 steel (wt.%, base Fe).

C	Cr	Mn	Mo	Nb	V	W	Ni	N	Si	Ta	Ce	Ti	B	Zr
0.16	11.17	0.74	0.01	0.01	0.25	1.13	0.03	0.04	0.33	0.08	0.15	0.05	0.006	0.05

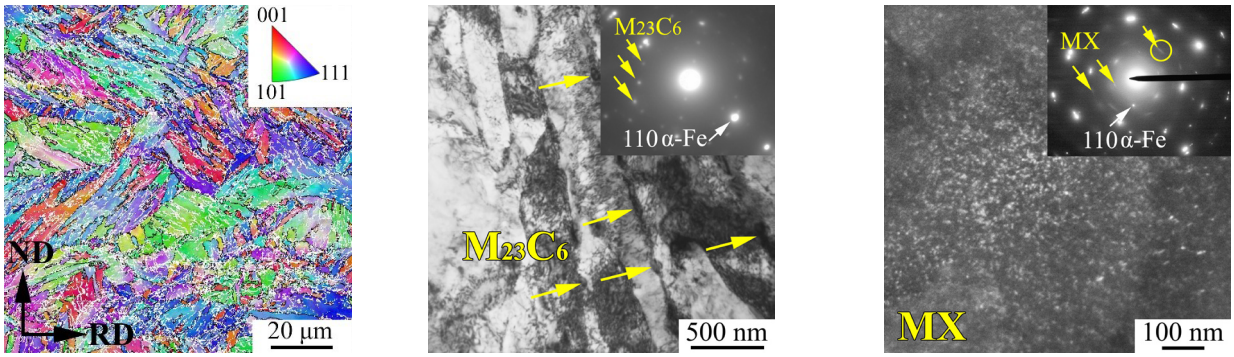

a b c

Fig. 2. (Color online) Microstructure of EK-181 steel after HTMT: EBSD (Electron Backscatter Diffraction) orientation map (high- and low-angle boundaries denoted by black and white lines, respectively) (a); bright-field electron microscopic image of martensitic lath structure with carbides $M_{23}C_6$ (b); dark-field electron microscopic image in the reflection of MX-type carbonitrides (c). RD — the rolling direction, ND — the direction normal to the rolling plane.

(from −7 to −15°C) relative to THT. At the same time, there is also an increase in the upper shelf energy (USE) from ≈54 J/cm^2 after THT to ≈65 J/cm^2 after HTMT (Fig. 3).

Figure 4 shows SEM micrographs of the impact test sample fracture surfaces of steel EK-181 after THT and HTMT tested in [15] in the temperature range from −186 to 100°C. It can be seen from these figures that the test temperature has a significant effect on the macrostructure of the fractures after both treatment modes.

At T = 28°C, the fracture surface of the samples after THT consists of the crack initiation zone (IZ), the fibrous zone (FZ), the unstable fracture zone (UFZ), the shear lip zone (SLZ) and the final fracture zone (FFZ, Figs. 4 a, 5 a).

In the IZ, FZ, SLZ, FFZ regions, fracture occurs mainly by the mechanism of ductile transcrystalline fracture through the formation, growth and coalescence of micropores (Fig. 5 b). Since micropores originate on inhomogeneities (particles of the second phases, segregations of dissolved

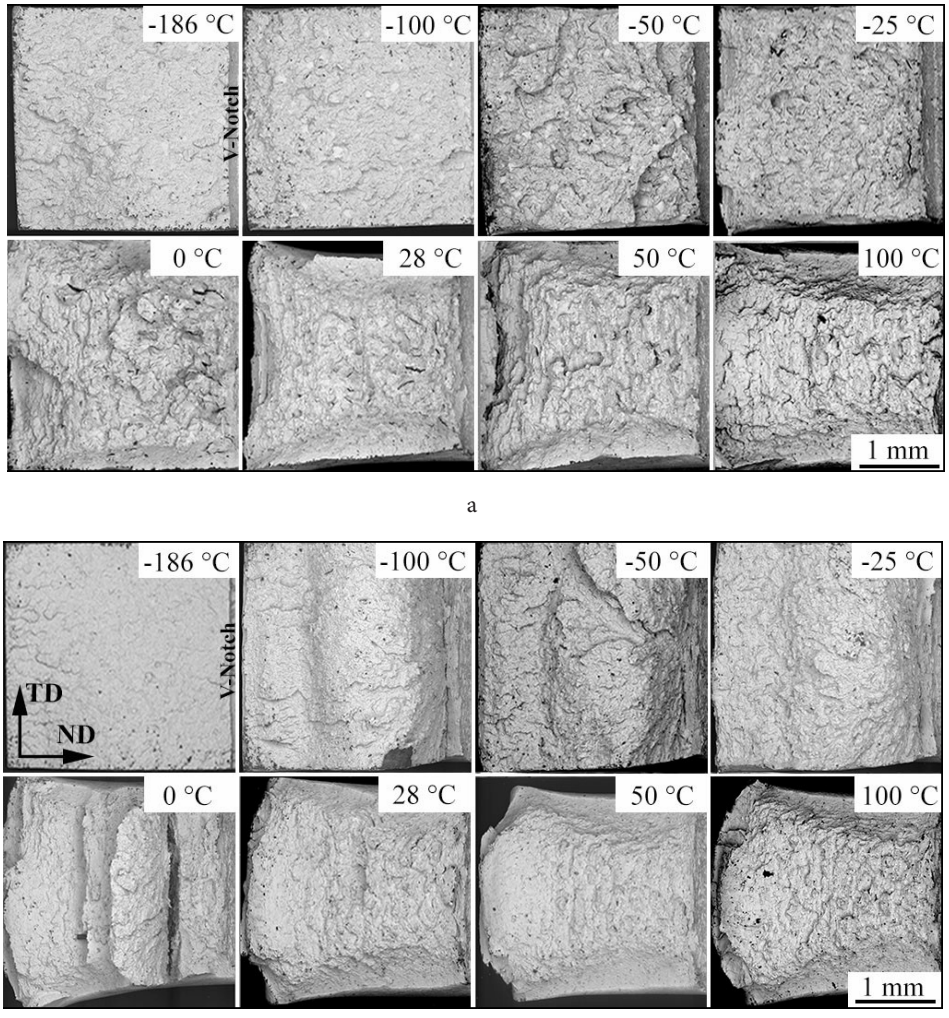

Fig. 4. Fracture surface of Charpy impact test samples after THT (a) and HTMT (b) destroyed at different temperatures.

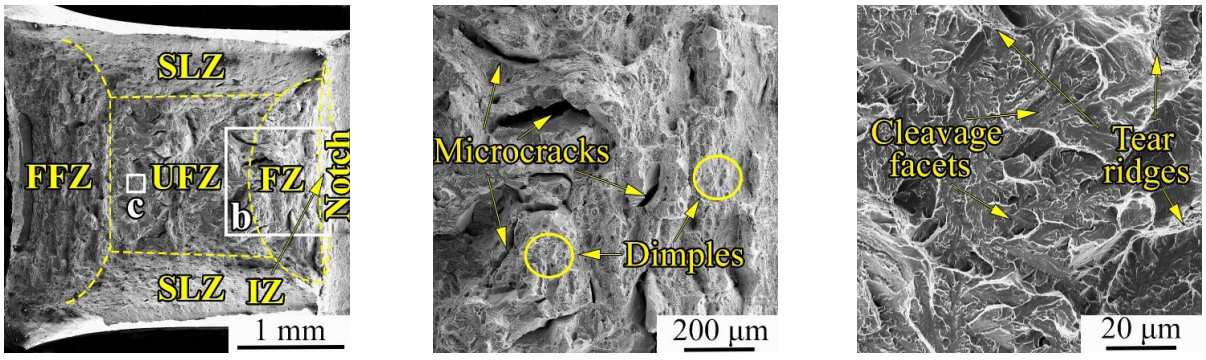

Fig. 5. SEM images of fracture surfaces of the samples after THT broken during impact test at 28°C (a) and magnified areas marked by white squares at Fig. 5 a (b, c). IZ — crack initiation zone, FZ — fibrous zone, UFZ — unstable fracture zone, SLZ — shear lip zone, FFZ — final fracture zone.

elements, grain boundaries), the size and distribution of the latter have a significant impact on the development of this type of fracture [16–18].

A ductile stable crack propagation occurs in the FZ region. Most of the dimples here have submicron dimensions (Fig. 5 b). In addition to them, the fractures contain single dimples with a diameter of several (up to 10 μm) micrometers. At the same time, most of the dimples have rounded shapes. In addition, multiple microcracks were found in the FZ, the walls of which also contain ductile fracture dimples (Fig. 5 b). Probably, there occurs a local intercrystalline ductile fracture.

Elongated dimples (parabolic shape) are formed in the near-surface zones (SLZ, FFZ) of the impact samples of steel EK-181. Here, in conditions of an increased vacancy concentration and the highest possible dislocation mobility, a plane-stressed state is formed [5], which contributes to the ductile propagation of a crack.

In the UFZ, a brittle fracture by the quasi-cleavage mechanism dominates (Fig. 5 c). There are characteristic features of this destruction — a river pattern, a fan-shaped pattern, and cleavage tongues. Quasi-cleavage crack propagation here is transcrystalline (transgranular) with respect to the prior austenite grain boundaries, martensite packets and ferrite grains. Cleavage cracks originate in the places where crystallographic sliding is difficult — at grain boundaries, at the intersections of twins, sliding planes, on inclusions and particles of the second phases [17].

The fracture surfaces in this region (UFZ) consist of quasi-cleavage facets. Note that many of them have an elongated shape, which, in our opinion, refers to the elongated and flattened shape of the steel grains. It is not always possible to detect clear boundaries between adjacent facets. Therefore, it is difficult to determine their exact dimensions. According to the analysis of fractograms, the transverse dimensions of the facets are commonly within ≈10 μm (Fig. 5 c).

It should be noted that on the fracture surface of samples after HTMT tested at room temperature (T = 28°C) there is no zone of unstable crack propagation. This correlates with the higher, relative to THT, values of impact toughness at this temperature (Fig. 3). In the structural state after HTMT, a pronounced UFZ appears at 0°C.

With a decrease in the deformation temperature after both treatments, the UFZ expands and the remaining areas decrease accordingly. This leads to an increase in the area fraction of brittle fracture (Figs. 3, 4). There are also separate areas of intercrystalline brittle fracture in this zone. For example, Fig. 6 b shows the facets of brittle intergranular fracture. However, in the UFZ we note the presence of multiple shear ridges containing small dimples (Fig. 6 b). They indicate the presence of local plastic deformation.

Thus, in the region of the ductile-brittle transition (from ≈0 to −50°C) the fracture surfaces of the impact samples contain elements of both brittle (quasi-cleavage facets) and ductile (numerous dimples) fracture. The steel is destroyed here by a mixed mechanism (Figs. 4, 6 b, e).

On the lower shelf of the impact toughness temperature curve, UFZ occupies almost the entire fracture surface. The shear lips zone and final fracture zone are practically absent. Therefore, there is no arrest of unstable crack propagation. Fracture at T = −186°C occurs by the mechanism of a transcrystalline quasi-cleavage. Multiple quasi-cleavage facets are observed on the fracture surfaces (Figs. 4, 6 a, d).

At the temperatures corresponding to the upper shelf of the temperature curve of the impact toughness (50–100°C), on the contrary, UFZ disappears. The steel (both after THT and after HTMT) is destroyed by the ductile mechanism

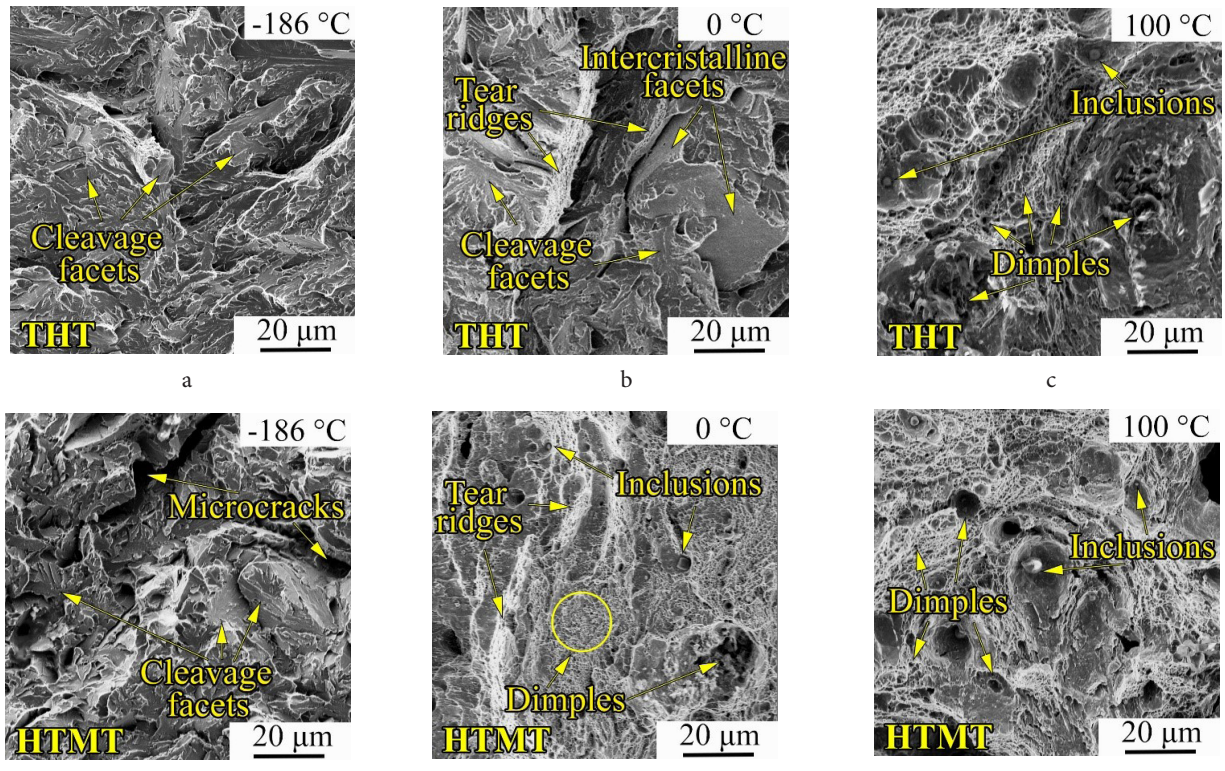

Fig. 6. SEM images of central part of fracture surfaces of the impact samples after THT (a – c) and HTMT (d – f).

of dimple fracture (Figs. 4, 6 c, f). The size of the dimples is mainly ≤1 μm similarly to that at room test temperature (Fig. 6 c, f). At the same time, the number of larger dimples increases in comparison with room and lower temperatures. Their sizes here can reach ≈40 μm. In some cases, slip marks are found on the walls of such dimples. Globular inclusions with different diameters are often present on the dimple bottoms (Figs. 6 c, f). Probably, most micropores originate on $M_{23}C_6$ carbide particles. Void initiation occurs either by separation of the inclusion-matrix interface or by cracking of the particles.

The largest particles observed in the fractures (up to 5 μm in diameter), according to the data of elemental microanalysis, are carbonitrides of the MX type enriched with Ta and Ti. They are probably formed at the stage of metallurgical operations. Due to their size and high hardness, such particles are strong stress concentrators during deformation of the samples. The pores on them form due to the incompatibility of the plastic deformation of the particle and the matrix. Note also that the volume fraction of the coarse particles discussed in the steel EK-181 is quite small (<1%).

Furthermore, we estimated the fracture areas occupied by ductile and brittle areas (Fig. 3). As can be seen from Fig. 3, the temperature of the steel FATT, at which the proportions of ductile and brittle fracture are the same (50/50%), is close to the ductile-brittle transition temperature (DBTT) determined from the impact tests (Fig. 3). Thus, the FATT value for the state after THT is ≈−3°C, after HTMT — ≈−14°C (Fig. 3).

HTMT has a significant effect on the character of the impact sample destruction, in comparison with THT. It leads to a shift (decrease) of the temperatures where the unstable crack propagation appears, relative to THT. In addition, HTMT also causes the delaminations in the temperature region of the ductile-brittle transition (Figs. 4, 7). These delaminations are formed in the planes parallel to the rolling plane (RD-TD planes), that is, perpendicular to the main crack propagation direction (Fig. 7). Delamination is an intercrystalline fracture along weak interfaces (between grains with high-angle boundaries) formed as a result of hot plastic deformation [18–22]. At the same time, we note that even at −50°C, there are signs of ductile dimples fracture on the delamination walls.

In the literature, the above-discussed delaminations are classified as the crack-arrester delaminations [18, 21, 22]. Many authors note that their presence is typical for the considered geometry (orientation of the long axis and V-notch of the Charpy-type samples with respect to the direction and plane of rolling) of hot-rolled samples of the ferritic-martensitic steels and leads to an increase in their impact toughness relative to other sample types [21, 23].

Coming across a delamination, the main crack can deviate (Fig. 7 b). Its path becomes zigzag. The fracture branching angle is often ≈90° or ≈120° (Fig. 7 b). In our opinion, this may be due to the presence of a crystallographic texture in the material after HTMT. However, this question requires further detailed research.

The V-notch of the impact samples is a strong stress concentrator. A triaxial stress state is created at the notch tip. It favors an easy generation of microcracks, which combine into a main crack. Apparently, the occurrence of delaminations due to slowing down (blunting) of the main crack and growth of its path increases the energy consumption of the fracture process. Thus, the presence of delaminations increases the amount of absorbed impact energy.

In the state after THT, the path of the main crack is practically rectilinear and there are no such fracture features (delaminations) (Fig. 7 a).

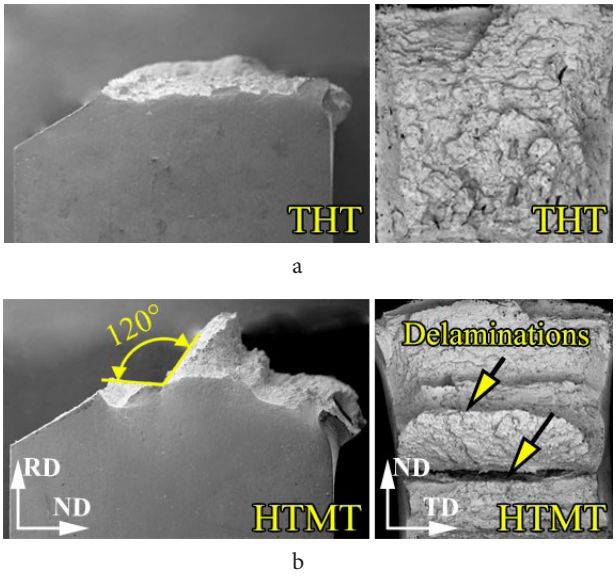

Fig. 7. SEM images of the lateral side and fracture surface of the impact samples after THT (a) and HTMT (b), fractured at 0°C.

4. Conclusions

Comparative fractographic investigations of the fracture features in the temperature range from −186 to 100°C of the impact samples of low-activation ferritic-martensitic steel EK-181 after a high-temperature thermomechanical treatment and traditional heat treatment have been carried out. Based on the results obtained, the following conclusions are made:

After both treatment modes, with a change in the impact test temperature, the fracture mechanism of steel EK-181 changes. At the temperatures corresponding to the upper shelf of the temperature curve of the impact toughness, it is destroyed by the mechanism of ductile dimple transcrystalline fracture. With a decrease in the temperature (in the region of the ductile-brittle transition), the fracture has a mixed character — there appears a zone of brittle unstable crack propagation; it increases in size and so does the brittle facture area fraction. When the temperatures corresponding to the lower shelf of the temperature curve of the impact toughness are reached, the areas of ductile fracture disappear. The fracture occurs by a transcrystalline quasi-cleavage with some local areas of intercrystalline brittle fracture.

The temperature of a transition to the brittle state, at which the fractions of ductile and brittle area fracture are the same, is close to the DBTT temperature determined from the impact tests after both treatments. After THT, DBTT ≈ −7°C, FATT ≈ −3°C; after HTMT: DBTT ≈ −15°C, FATT ≈ −14°C.

HTMT has a significant effect on the character of the impact sample fracture, in comparison with THT. It leads to a

decrease in the temperature of the brittle fracture development and the formation of crack-arrester delaminations in the planes parallel to the rolling plane in the ductile-brittle transition region of the steel. The presence of this type of delamination, which contributes to an increase in the values of absorbed impact energy, is one of the factors for increasing the impact toughness and reducing the temperature of the ductile-brittle transition of the steel.

Acknowledgements. This study was funded by the Russian Science Foundation; Project No. 21-79-00231, https://rscf.ru/project/21-79-00231/.

References

1. R.G. Odette, S.J. Zinkle. Structural Alloys for Nuclear Energy Applications. Elsevier (2019) 655 p. Crossref
2. R.L. Klueh, A.T. Nelson. J. Nucl. Mater. 371 (1-3), 37 (2007). Crossref
3. F.A. Garner. Comprehensive Nuclear Materials 2nd edition. 3, 57 (2020). Crossref
4. J. Vivas, D. De-Castro, E. Altstadt, M. Houska, D. San-Martín, C. Capdevila. Mater. Sci. Eng. A. 793, 139799 (2020). Crossref
5. H. Mohrbacher. Metals. 8 (4), 234 (2018). Crossref
6. P. Fernandez, J. Hoffmann, M. Rieth, A. Gomez-Herrero. Mat. Charact. 180, 111443 (2021). Crossref
7. V.M. Chernov, G.N. Ermolaev, M.V. Leont'eva-Smirnova. Tech. phys. 7, 985 (2010). Crossref
8. A.N. Tyumentsev, E.G. Astafurova, I.Y. Litovchenko, V.M. Chernov, M.V. Leont'eva-Smirnova, N.A. Shevyako. Tech. phys. 1, 985 (2012). Crossref
9. R. Esterl, M. Sonnleitner, I. Weißensteiner, K. Hartl, R. Schnitzer. J Mater Sci. 54, 12875 (2019). Crossref
10. H.L. Haskel, E. Pauletti, J.P. Martins, A.L.M. de Carvalho. Mat. Res. 17 (5), 1238 (2014). Crossref
11. I. Litovchenko, K. Almaeva, N. Polekhina, S. Akkuzin, V. Linnik, E. Moskvichev, V. Chernov, M. Leontyeva-Smirnova. Met. 12, 79 (2022). Crossref
12. I.Yu. Litovchenko, N.A. Polekhina, A.N. Tyumentsev, E.G. Astafurova, V.M. Chernov, M.V. Leontieva-Smirnova. J. Nucl. Mater. 455, 665 (2014). Crossref
13. N.A. Polekhina, I.Yu. Litovchenko, A.N. Tyumentsev, D.A. Kravchenko, V.M. Chernov, M.V. Leontyeva-Smirnova. Tech. Phys. 62 (5), 736 (2017). Crossref
14. N.A. Polekhina, I.Yu. Litovchenko, K.V. Almaeva, A.N. Tyumentsev, V.M. Chernov, M.V. Leontyeva-Smirnova. Inorg. Mater.: Applied Research. 13 (5), 1247 (2022). Crossref
15. N.A. Polekhina, V.V. Linnik, K.V. Almaeva, I.Yu. Litovchenko, A.N. Tymentsev, E.N. Moskvichev, V.M. Chernov, M.V. Leontyeva-Smirnova, N.A. Degtyarev, K.A. Moroz. Rus. Phys. J. 64 (12), 2225 (2022). Crossref
16. A. Pineau, A.A. Benzerga, T. Pardoen. Acta Mater. 107, 424 (2016). Crossref
17. G.V. Klevtsov, L.R. Botvina, N.A. Klevtsova, L.V. Limar. Fractodiagnostics of destruction of metallic materials and designs. Moscow, MISiS (2007) 264 p. (in Russian)
18. T. Maeda, S. Okuhata, K. Matsuda, T. Masumura, T. Tsuchiyama, H. Shirahata, Y. Kawamoto, M. Fujioka, R. Uemori. Mater. Sci. Eng. A. 812, 141058 (2021). Crossref
19. P. Modak, A. Ghosh, N. Rarhi, Vinod Kumar, R. Balamuralikrishnan, D. Chakrabarti. Metal News. 19, 21 (2016).
20. Y. Niu, S. Jia, Q. Liu, S. Tong, B. Li, Y. Ren, B. Wang. Mater. 12, 3672 (2019). Crossref
21. T. Inoue, Y. Kimura. Mater. 15, 867 (2022). Crossref
22. A. Ghosh, S. Patra, A. Chatterjee, D. Chakrabarti. Metall. Mater. Trans. A. 47 (6), 2755 (2016). Crossref
23. A. Chatterjee, A. Ghosh, A. Moitra, A.K. Bhaduri, R. Mitra, D. Chakrabarti. Int. J. Plast. 104, 104 (2018). Crossref